HAADF-STEM and DFT investigations of the Zn-containing β” phase in Al-Mg-Si alloys

Takeshi Saito[1,*], Flemming J.H. Ehlers[1], Williams Lefebvre[2], David Hernandez-Maldonado[2], Ruben Bjørge[1,a], Calin D. Marioara[3], Sigmund J. Andersen[3], and Randi Holmestad[1]

[1]Department of Physics, Norwegian University of Science and Technology (NTNU), N-7491 Trondheim, Norway
[2]Université de Rouen, GPM, UMR CNRS 6634 BP 12, Avenue de I'Université, 76801 Saint Etienne du Rouvray, France
[3]SINTEF Materials and Chemistry, N-7465 Trondheim, Norway

*Corresponding author
Email: takeshi.saito@ntnu.no
Phone number: +47 73 59 07 30
Postal address: Høgskoleringen 5, Realfagbygget, 7491 Trondheim, Norway

[a]Present affiliation: SINTEF Materials and Chemistry, N-7465 Trondheim, Norway

Abstract

The Zn-containing β” phase in Al-Mg-Si alloys has been investigated by aberration corrected high angle annular dark-field scanning transmission electron microscopy (HAADF-STEM), combined with density functional theory (DFT) calculations. The mean intensity of one Si site of the β” phase is higher than the other Si sites, suggesting partial Zn occupancy. DFT studies support that this Si site is competitive for Zn incorporation. While HAADF-STEM image simulations show an influence of the Zn distribution along the β” main growth direction, total energy calculations predict a weak Zn-Zn interaction. This suggests that Zn atoms are not clustering, but uniformly distributed along the atomic columns. The Zn incorporation has a weak influence on the β” phase where Zn is admitted as a “defect” according to the DFT studies.

Keywords: aluminum alloys; precipitate; STEM HAADF; DFT; atomic structure; image analysis

1. Introduction

Al-Mg-Si alloys are heat-treatable materials used in many industrial applications on the basis of their characteristic properties: high strength-to-weight ratio, good formability and corrosion resistance. The main property of these heat-treatable materials is a significant increase in hardness during a final isothermal heat treatment (artificial aging) at an adequate temperature and time. This is due to the formation of large numbers of nano-sized semi-coherent metastable precipitates, hindering dislocation movement. The precipitates form from a super saturated solid solution (SSSS) and are controlled by the alloy composition and the thermo-mechanical history. The materials strength ultimately depends on the precipitate structure and the microstructures they produce (sizes, numbers and orientations). Further, composition, morphology and aspect ratio for a precipitate may be affected by small amounts of a different type of solute atoms. This

could be triggered by direct incorporation of these additional solute atoms in the existing precipitate, either in the bulk (change of cell dimensions) or at the interface (change of interfacial energies). Such alloy modifications are of growing interest due to specific industrial requirements for materials properties and focus on recycled aluminium.

The precipitation sequence of Al-Mg-Si alloys is as follows [1-9]:

$$\text{SSSS} \rightarrow \text{atomic clusters} \rightarrow \text{GP zones (pre-}\beta\text{”)} \rightarrow \beta\text{”} \rightarrow \beta\text{', U1, U2, B'} \rightarrow \beta, \text{Si} \quad (1)$$

The U1, U2 and B' phases are also known as Type A, Type B and Type C, respectively [10].

The β” phase is the most important metastable phase encountered together with GP zones, leading to the finest microstructure at peak hardness condition [1]. The monoclinic structure (space group C2/m) of the β” phase, described in Figure 1 (a) and Table 1, was identified more than a decade ago [2, 9]. By contrast, the β” composition has been widely discussed [3, 11-15]. The β”/Al matrix interfaces are coherent, with {130}Al and {320}Al as habit planes. The orientation relationships with the face-centred cubic (fcc) Al matrix are:

$$[230]\text{Al} \,//\, [100]\beta\text{”}; [001]\text{Al} \,//\, [010]\beta\text{”}; [-310]\text{Al} \,//\, [001]\beta\text{”}. \quad (2)$$

The lattice misfits along these directions are in the order of 3.8%, 0% and 5.3%, respectively [2, 9] from which a needle shaped precipitate, directed along [010]β”, results. Recent extensive experimental atom probe tomography (APT) studies suggested [3, 12, 13] that the Mg/Si ratio is close to 1.1 which differs from the originally proposed β”-Mg_5Si_6 phase. Both experimental studies and theoretical density functional theory (DFT) calculations [3, 12-14] have supported the $Mg_5Al_2Si_4$ composition, most likely the β” configuration in Figure 1 (a). The most recent DFT calculations [14] deduced very weak formation enthalpy differences for β”-$Mg_{5+x}Al_{2-x}Si_4$ ($-1 < x < 1$). Further, the β” phase could have compositional variations within a single precipitate, as suggested by the most recent experimental study [15]. These results imply the possibility of a strong sensitivity for the β” phase composition, aspect ratio and ultimately the microstructure, to incorporation of “foreign” solute atom types.

In the present work, we investigate the incorporation of Zn in β”, utilizing a series of experimental and theoretical methods, from the perspective of a general analysis of foreign solute atom types in this phase. It has previously been demonstrated [16], by high-angle annular dark-field scanning transmission electron microscopy (HAADF-STEM), that Zn is confined to the Si3/Al sites of the β” phase, see Figure 1 (b). The contrast of these Zn-containing atomic columns was weak, which indicates a low Zn partial occupation on the site [16]. Our main interest in this work is how to clarify, to the largest possible degree, the state of “a well-known phase with foreign solute atom types” – here, the β” phase with the Zn incorporation.

It is well known that information acquired from HAADF-STEM images is limited due to the “projection” of the 3-dimensional (3D) atomic structure and complicated scattering mechanisms [17, 18]. We aim at circumventing this limitation by utilizing both a statistical analysis and simulations of the HAADF-STEM intensities, as well as DFT calculations. This attempt should serve to highlight the present limitations of the general structural analysis, as well as the key areas where further investigations are needed.

2. Experimental details and methodologies

2.1. Materials and HAADF-STEM images

An alloy with measured composition Al-0.52Mg-0.38Si-0.42Zn (at.%) was prepared by extrusion from cast billets. This composition is close to the commercial 6060 Al alloy, except for the Zn addition. Other impurities are below 0.01 at.%. The alloy was solution heat treated at 540°C for 1 h, kept for 4 h at room temperature and isothermally heat treated at 185°C for 12 h. This heat treatment procedure gives a peak hardness condition. The preparation and heat treatment are identical to the previous work [16].

HAADF-STEM specimens were prepared by electropolishing with a Tenupol 5 machine (Struers, Denmark). The electrolyte consisted of 1/3 HNO_3 in methanol and the solution was kept at a temperature between -20°C and -35°C. In order to reduce contamination during observation, all specimens were ion-milled by a precision ion polishing system (PIPS Gatan). In addition, all specimens were plasma cleaned before HAADF-STEM imaging in order to reduce the effect of contamination, using a Model 1020 Plasma Cleaner (Fischione Instruments). The HAADF-STEM images were taken by a spherical aberration (Cs) probe-corrected JEOL ARM200F STEM with a Schottky field emitter operating at 200 kV. The probe size was 0.1 nm. The collection angle of the HAADF detector was in the range of 45-150 mrad. The thickness of the specimen was near 50 nm. The HAADF-STEM technique provides atomic number (Z) contrast with the intensity proportional to $Z^{1.7\text{-}1.9}$ [17, 18]. This enables to distinguish the heavier Zn (Z_{Zn} = 30) enriched atomic columns from those containing only Mg (Z_{Mg} = 12), Al (Z_{Al} = 13) and Si (Z_{Si} = 14) in the precipitate structures.

2.2. Analysis of HAADF-STEM intensity by a statistical approach

The intensities of atomic columns of the precipitate examined were estimated using a statistical analysis [19, 20]. The HAADF-STEM intensity $I(\boldsymbol{R})$ can be approximated as a convolution of an object function and a probe function as follows [18]:

$$I(\boldsymbol{R}) = O(\boldsymbol{R}) \otimes P(\boldsymbol{R}) . \qquad (3)$$

Here, $\boldsymbol{R}$ is the position of the STEM probe, $O(\boldsymbol{R})$ is the object function and $P(\boldsymbol{R})$ is the probe function. The probe function represents the intensity distribution of the convergent scanning beam, which depends on acceleration voltage, objective aperture, convergence angle and defocus [18]. On the other hand, the object function describes the scattering, related to the projected potential of atomic columns. This function is peaked at the atomic column positions and can be modelled as a superposition of Gaussian peaks [19, 20]. The scattered intensity for an atomic column is expected to be identical for columns with the same chemical composition. In this manner, histograms of the estimated peak intensity of the atomic columns can be drawn [19]. This methodology [19, 20] has been developed to count the atoms in nano-sized particles from HAADF-STEM images. We here applied the method to identify the atom types in the various columns, assuming the same number of atoms in each column of a precipitate. This approach has recently been followed to investigate the β” phase without Zn incorporation, deducing atomic column types [15].

Following the methodology proposed by van Aert et al [19, 20], integrated column intensities were measured for each atomic column in the experimental images (i.e. without any filtering). Histograms of column intensities were then fitted with a Gaussian "mixture model", using a statistical analysis in which the amounts of Gaussian components [19, 20] are estimated from the variation of the ICL (integrated classification likelihood) criterion. This approach enables the intensity distribution of each atomic column to be estimated and discussed.

2.3. HAADF-STEM image simulations

In order to clarify how a partial occupancy of Zn at the Si3/Al site in the β" phase influences the HAADF-STEM intensity, three different Zn occupancies, 0%, 5% and 10% on this site were simulated. The composition of the β" phase was assumed to be $Mg_5Al_2Si_4$. In addition, to investigate how the intensity varies with Zn distribution along a precipitate needle, three different distributions along the electron beam direction were considered: even distribution throughout the column, and top and bottom Zn enrichments (see Figure 2). In this manner, we can extract 3D information on the precipitate atomic structure from the projected HAADF-STEM images.

The HAADF-STEM image simulations were conducted using the frozen phonon multislice program provided by the QSTEM package [21] with slice thickness of 0.205 nm (half a unit cell, see Table 1). The convergence semi angle of the electron probe was 20 mrad and the HAADF collector angles were between 45 and 150 mrad. These values were the same as in the experiment. The simulated structures were assumed (see Table 1) to adopt the experimentally reported [2] β" cell dimensions, regardless of Zn content and distribution. The HAADF-STEM images were calculated for every two slices. Each simulation was averaged over 30 frozen phonon configurations. The chosen Debye-Waller factors for each site matched those of the elemental phases at 300 K: 0.8333, 1.8837, 0.5261 and 1.1782 $Å^2$ for Al, Mg, Si and Zn, respectively [22].

2.4. Density functional theory (DFT) calculations

The DFT [23, 24] calculations for the Zn containing β" phase have three key purposes. We attempt to:

- Compute the energy gain for a Zn atom incorporated in β" (named "replacement energy" below), as obtained relative to having this atom in solid solution (SS).
- Clarify the level of Zn induced changes to the β" composition.
- Elucidate the strength of Zn-Zn interactions in β" (and thus, in turn, the expected degree of Zn clustering in the precipitate).

To capture the state of Zn in the precipitate, calculations on a bulk β" system are needed. Due to the expected low Zn occupancy in β", we modelled the precipitate using supercells, comprising $N_a \times N_b \times N_c$ primitive β" unit cells (see Figure 1(a)) along $\mathbf{a}_{\beta"}$, $\mathbf{b}_{\beta"}$ and $\mathbf{c}_{\beta"}$, respectively. Initially, we incorporated one Zn atom in a $1 \times 4 \times 1$ cell, testing the preference for each non-equivalent site in β", in a manner to be described below. To examine Zn clustering tendencies, we introduced a second Zn atom on an equivalent site, varying the Zn-Zn separation. Those studies involved both the $1 \times 4 \times 1$ cell as well as $1 \times 2 \times 2$ and $2 \times 2 \times 1$ cells. For the description of Zn in SS, we included one Zn atom in a 108 atom fcc Al supercell, comprising $3 \times 3 \times 3$ conventional fcc unit cells.

To accommodate β” configurations with space group symmetry lower than C2/m in calculations, we treated all atom sites Ξ for the Zn-free structure (labelled β''_0 for brevity below) as formally non-equivalent. This yielded 11 different sites within the primitive cell of Figure 1 (a). The drive for Zn incorporation on any of these sites was addressed as follows: whenever a solute atom was present at site Ξ in β''_0, we introduced an “artificial” Al defect here, for each primitive cell making up the full supercell (four Al atoms introduced in total). We then considered two possible scenarios:

- One Zn atom removed from the fcc Al supercell and incorporated on site Ξ, with the Al atom present here expelled to the Al matrix.
- The same substitution process examined for the solute atom occupying site Ξ before the introduction of the artificial Al defects.

In this manner, we probe not only the drive for Zn incorporation on each given site in β”, but also *the level of competition* with the solute atom most likely occupying this site when no Zn is present in the alloy. Labelling the incorporation of a given atom X on site Ξ as “{X → Ξ}”, the system enthalpy change $\Delta H(\beta''_0;\ X \rightarrow \Xi)$ due to one of the above described substitution processes may be written as:

$$\Delta H(\beta''_0;\ X \rightarrow \Xi) = H(\beta''_0;\ 3 \times \{Al \rightarrow \Xi\};\ 1 \times \{X \rightarrow \Xi\}) + H(\text{fcc Al}) - H(\beta''_0;\ 4 \times \{Al \rightarrow \Xi\}) - H(\text{fcc Al};\ 1 \times \{X \rightarrow S\}). \quad (4)$$

Here, *H* denotes the calculated enthalpy for the system described in parenthesis (first argument: host material; remaining arguments: replacement processes), with X specifying the solute atom incorporated in the precipitate and S denoting a substitutional site in the Al matrix. Following [3, 14], we considered three different (energetically competitive) β''_0 configurations; $Mg_4Al_3Si_4$ (Al on Mg1, Si3 sites in Figure 1 (a)), $Mg_5Al_2Si_4$ (Al on Si3 sites), and Mg_6AlSi_4 (Al on one Si3 site). For sites Ξ hosting Al in β''_0, the replacement processes “{Al → Ξ}” have no practical effect. However, even for this situation we considered incorporation of the most likely solute atom Mg/Si on site Ξ for comparison with the Zn incorporation.

All computational studies were performed at 0 K, employing Vanderbilt ultrasoft pseudopotentials [25] as implemented in the plane wave (PW) based Vienna Ab initio Simulation Package (VASP) [26, 27]. For the description of the exchange-correlation functional, the Perdew-Wang generalized gradient approximation [28] was used. The chosen PW cut-off in simulations was 234 eV, with (12, 6, 14) Monkhorst-Pack [29] *k*-point grids used for the 1 × 4 × 1 β” supercell, and compatible grids for other cells. Generally, all structural parameters (cell dimensions, basis vector angles and atomic positions) were relaxed. The use of enthalpies over formation energies *E* in eq. (4) relates to our neglecting the influence of the (small) pressure-volume (*PV*) term distinguishing these quantities.

3. Results

3.1 HAADF-STEM intensity distribution of atomic columns by statistical analysis

Figure 3 shows an unprocessed HAADF-STEM image of a β” precipitate cross-section taken along <001>Al and the corresponding average HAADF-STEM intensity map. The intensity map shows thickness variations over the specimen, deduced by integrating the intensity over a square area larger than the size of a projected column. This means that each dot overlaid a column in

Figure 3 (b) is a centre, with colour representing the (average) intensity of the surrounding area. Figure 4 shows the intensity map of the Si3/Al sites, and intensity distributions for each Mg and Si site in the precipitate. The following observations can be made from Figures 3 and 4:

- The intensity map shows a strong intensity variation, reflecting thickness variations of the scanned area. In addition, the intensity from the bulk precipitate is relatively lower than the Al matrix. This could be attributed to elastic lattice strain in the precipitate [30]. Here, it cannot be excluded that the actual thickness of the bulk precipitate and the Al matrix might be different due to the results of specimen preparation.
- While the intensity distributions for the Mg sites are similar to each other, those for the Si sites show clear differences among the sites. The mean intensity of the Si3/Al sites is clearly higher than other Si sites. This is in good agreement with a partial occupation of Zn on the Si3/Al sites.
- Intensities for the Si3/Al sites are lower *close to* the interfaces along [230]Al; the higher intensity comes from the bulk Si3/Al sites, not from either *near* or *at* interfaces along [230]Al. Interestingly, this tendency appears weaker for the interfaces along [-310]Al.
- A small part of area on the interface along [-310]Al is non-systematically brighter than the bulk (bottom part of the precipitate shown in Figure 4(a)). This might be due to local Zn enrichment at the precipitate/matrix interface. Similar observations were made for disordered precipitates examined in previous work [16].
- The widths of the intensity distributions for the Si2 and Si3/Al sites exceed that of the Si1 site.

3.2 Simulated HAADF-STEM intensity

Figure 5 shows the simulated intensities for the Si3/Al site as a function of thickness for 5% and 10% Zn occupancies with different Zn distributions along the electron beam direction as shown in Figure 2. As a reference, the intensity for all Si sites (Si1, Si2 and Si3) in the β" phase *without* Zn occupation are also shown in Figure 5. As expected, the intensity increases with increasing specimen thickness. Since the intensity variation in a HAADF-STEM image is approximately linear with increasing thickness [18], an intensity gradient was deduced by linear interpolation. Table 2 lists the fitted intensity gradients of Figure 5. The following observations can be made from Figure 5 and Table 2:

- The intensity differences between Si sites are negligibly small, compared to the intensity variations in the case with partial Zn occupation.
- Regardless of the Zn distribution imposed along the electron beam direction, the presence of Zn increases the intensity.
- The intensity gradient with respect to thickness increases with Zn occupancy for all distributions.
- Differences among the intensity gradients are encountered depending on the Zn distribution along the column. These variations are weak in 5% Zn occupancy. For 10% Zn occupancy, the variation has increased. In both cases, Zn top enrichment yields higher interties. We note that deviations from liner behavior in the actual curves make this scatter most pronounced at realistic specimen thickness (above ~40 nm). None of the selected Zn distributions can be excluded as unphysical based on the information in Figure 3 (a). These results indicate that determining the level of partial Zn occupancy from HAADF-STEM image intensities is not a trivial problem.

3.3 Calculated Zn replacement energies

Figure 6 shows the calculated energies $\Delta H(\beta''_0;\ X \rightarrow \Xi)$ obtained when considering incorporation of X = Zn/Mg/Si on the various sites Ξ in an initially Zn-free precipitate β''_0, as described with eq. (4). Given the chosen supercell sizes (see section 2.4), the examined Zn occupancy is 12.5% for all sites but Mg1, where the occupancy is twice as high. In the presentation of the data, two simplifications were made: firstly, for the Si3/Al site in Mg_6AlSi_4, Zn (Mg) was only incorporated on the Al bearing (Mg bearing) site. Secondly, whenever symmetry breaking produced more than one energy for a selected case in Figure 6, only the lowest energies were included. This latter simplification had no significant influence on the results outlined below. The following observations can be made:

- For the Si3/Al sites, where Zn atoms were observed experimentally, theory predicts weak binding (–0.18 eV/Zn atom or higher), with little variation for the three different β''_0 configurations and a minimum at the $Mg_5Al_2Si_4$ composition.
- Compared to Zn, Mg may occupy the Si3/Al sites at a similar energy gain, but with the Mg2, and Mg3 sites clearly favoured (-0.60 eV/Mg atom or lower).
- Compared to the Si3/Al site, Zn is predicted to bind more strongly on the Si1 and Si2 sites. Here, however, the "competing" Si atom is always binding more favourably. The only exception is the Si1 site in β"-$Mg_4Al_3Si_4$ where Zn incorporation is "competitive" (-0.51 eV/Zn atom vs -0.56 eV/Si atom).

Additional studies probing the level of Zn-Zn interactions in β" were performed only for Zn on Si3/Al sites in β"–$Mg_5Al_2Si_4$. The results suggest an almost complete indifference of the system energy to the Zn separation, implying that Zn is statistically distributed on the Si3/Al sites, as opposed to clustering, see Figure 7 (a). In further support of this conclusion, we note that the Zn replacement energy is unchanged compared to Figure 6, although the Zn concentration has been doubled.

The variation in the Zn replacement energy as a function of distance from the interface was also examined for Zn on the Si3/Al site in β"–$Mg_5Al_2Si_4$, see Figure 7 (b). The results indicate that Zn atoms are preferentially incorporated in *bulk* β" – *not close* to the interface.

4. Discussion

Although we see strong intensity variations due to thickness changes and elastic strain in the analysed β" precipitate, the statistical analysis of the HAADF-STEM image intensities in Figure 4 clearly indicates that the Si3/Al sites display a larger mean intensity compared to the Si1 and Si2 sites of the β" phase. In addition, the intensity distribution for the Si3/Al sites is broader. The HAADF-STEM image simulations in Figure 5 suggest that the intensity difference between Si sites is negligibly small, compared to intensity variations obtained with partial Zn occupations. Furthermore, DFT calculations predicted (see Figure 6) that the Si3/Al site should be the most favourable site for Zn incorporation in the β" phase. These results are in good agreement with a partial occupation of Zn atoms on the Si3/Al sites. Note that the intensity distribution for the Si2 sites is also broader and has slightly higher intensity than that for the Si1 sites. However, DFT calculations suggest that Zn is effectively less likely on the Si2 sites, compared to the Si3/Al (and even the Si1) sites. The broader intensity distribution for the Si2 sites might result from the Zn presence on the neighbouring Si3/Al sites, i.e. the increased intensity is due to electron channelling or cross-talk artefacts [31] between these sites. This could influence intensities along

<001>Al for a specimen thickness larger than 50 nm [32] – roughly the value in our studies. The intensity on the Mg sites was lower than on the Si sites. This suggests that the Mg sites are not occupied by Zn atoms, a conclusion also supported by the DFT calculations.

The higher intensities in Figure 4 (a) come from the *bulk* Si3/Al sites, as opposed to the precipitate/Al matrix interfaces and their vicinity, in case of the interface along [230]Al. We stress here that the average intensity in the bulk region (Figure 3(b)) is also higher than near the interface. This may be attributed to the elastic lattice strain on the β" precipitate, see the strain map in Ref. [15]. We cannot exclude, on the basis of the present work, that this strain is appreciably affecting the Zn binding energy reduction near the interface due to e.g. different bonding with surrounding atoms. In particular, we note that the DFT results in Figure 7 (b) do not predict differences in the Zn behaviour at the two interfaces. Further, the Zn binding energy in β" is always weak and as such susceptible to remaining errors in the calculations, e.g. finite temperature effects. To clarify whether strain or chemical effects are the more influential, DFT studies on strained supercells (following e.g. the methodology in Ref. [33]) as well as a closer experimental examination of compositional variations within the precipitate of Figure 3 (a) would be of interest.

The DFT results suggest (see Figure 6) that Zn on the Si3/Al site has only very weak preference for a particular β" composition. Since the Zn-free β" energy contours are equally weak, we cannot deduce solely from the above information how Zn may affect β" chemically. However, the results of Figure 6 also suggest that, in addition to the Si3/Al site, the Si1 site could be a competitive site for Zn incorporation in β"-$Mg_4Al_3Si_4$. Experimentally, no Zn on the Si1 site is observed. Further, the intensity distributions for the Mg sites in Figure 4 (b) are highly similar. Those two observations suggest that the analysed β" precipitate is unlikely to be dominated by local regions with the $Mg_4Al_3Si_4$ composition. Even with the significant theoretical incorporation of Zn in β", the cell dimensions and the structure of this phase change only weakly, preferably along the β" needle direction. It is inferred that Zn has a weak interaction with the β" phase, where it can be considered "a defect" preferentially located at the Si3/Al site.

The precise level of Zn occupancy at the Si3/Al site depends not only on the projected location within the precipitate, but also on the Zn distribution *along* the precipitate needle, as seen in the HAADF-STEM intensity analysis and simulations, respectively. The dependence on the distribution is weak at low Zn occupancy (5%). However, if the occupancy is 10% and the specimen thickness exceeds 40 nm, the intensities for top enrichment in Figure 5 are non-negligibly higher than the other distributions. The main reason for this dependence is a large influence of electron channelling (and/or de-channelling). In addition, the HAADF-STEM intensity generally depends on several factors: crystal structure and bonding, Debye-Waller factors, thickness and background intensity. These factors are decoupled influences on the HAADF-STEM intensity. As an example of the remaining complexities present here, a recent study [34] has shown that the HAADF-STEM intensity depends greatly on the Debye-Waller factors. Interestingly, the results indicated that the Z-contrast of the HAADF-STEM intensity was no longer truly valid, but depending on crystal structure and bonding. Other examples of complexities to be considered can be mentioned: an inhomogeneous HAADF detector intensity [35] and static disorder in atomic columns due to occupation of more than one type of atom in the column – so called "static atomic displacements" [36].

The DFT calculations indicate that the Zn-Zn interactions are weak for the Si3/Al site in the β" phase. Zn is inferred to be in favour of a uniform (statistical) distribution throughout the

Si3/Al site column, as opposed to the "clustering" tendencies reflected by the proposed top and bottom Zn enrichment in the HAADF-STEM image simulation, see Figure 2. In a previous work [16], Zn was shown to induce only a low increase in precipitate number density, compared to Zn-free alloys, consistent with the weak Zn influence proposed in the present study. Here, one thing may have to be considered: in principle, a new superstructure with different symmetry would arise if the Zn atoms were periodically distributed. The Zn distribution could be determined from an HAADF-STEM image taken in the direction normal to the precipitate needle (90 degrees tilted from the present orientation). As the needles are thin (less than 10 nm), however, observation may be difficult due to the huge projected atomic overlap with fcc Al in this direction.

As stated in the introduction, a key motivation in the present work has been to address the limits to the understanding of the state of "a well-known phase with foreign solute atom types". Our investigations have highlighted the example of Zn in β", which is characterized by its simple nature. Since Zn was shown from previous work [16] to occupy a single site (Si3/Al) in the precipitate, a greatly eased analysis was implied. The above discussed results have indicated that a combination of HAADF-STEM statistical analysis, HAADF-STEM image simulations and DFT calculations may provide highly useful information, not achievable by these techniques independently. HAADF-STEM statistical analysis in combination with DFT calculations suggests that Zn is confined to the Si3/Al sites and statistically distributed, with non-negligible consequences to the relation between Zn occupancy and intensity, as shown in HAADF-STEM image simulations. A combination of HAADF-STEM statistical analysis and simulations may quantify the Zn occupancy, with similar considerations applying to the β" composition. However, this is not straightforward because of thickness variations and decoupled factors influencing HAADF-STEM intensity as discussed earlier. To further clarify the state of the system, different experimental techniques, e.g. APT, may support the analysis to overcome the inherent limitation.

5. Conclusion

A combination of statistical analysis and simulations of HAADF-STEM intensities has been used along with DFT calculations to clarify the state of the Zn-containing β" phase in Al-Mg-Si alloys. Statistical analysis of HAADF-STEM intensities shows that the intensity distribution of the Si3/Al sites in the β" phase is broader, with markedly higher intensities, for atomic site columns presumed to contain Zn. DFT calculations support that these Si3/Al sites are preferential sites for Zn incorporation, with Zn admitted as a weakly binding "defect" in β". The occupancy of Zn atoms on the Si3/Al site depends on the region in the precipitate while the HAADF-STEM intensity varies as well with the Zn distribution along the precipitate needle. DFT calculations suggest a negligible Zn-Zn interaction, implying statistically distributed Zn in β". Quantification of the Zn content remains problematic, as a direct comparison of HAADF-STEM image simulations with experiment is complicated by several independent sources of errors. Improving the reliability of this comparison should be the main target of future work attempting a quantitative description of a precipitate accommodating low amounts of foreign solute atoms.

Acknowledgement

This research is supported by Hydro Aluminum and the Research Council of Norway though the bilateral KMB project: 193619 "The Norwegian-Japanese Al-Mg-Si Alloy Precipitation

Project". The authors would like to thank Dr. Olaf Engler, Hydro Bonn Germany, for composition measurement by inductively coupled plasma optical emission spectroscopy. W.L. acknowledges the Agence Nationale pour la Recherche for financial support through the Programme Jeune Chercheur – Jeune Chercheuse TIPSTEM. The DFT calculations were performed through access to NOTUR facilities.

References

[1] Edwards GA, Stiller K, Dunlop GL, Couper MJ. Acta Mater 1998;46:3893.
[2] Andersen SJ, Zandbergen HW, Jansen J, Træholt C, Tundal U, Reiso O. Acta Mater 1998;46:3283.
[3] Hasting HS, Frøseth AG, Andersen SJ, Vissers R, Walmsley JC, Marioara CD, Danoix F, Lefebvre W, Holmestad R. J Appl Phys 2009;106:123527.
[4] Marioara CD, Andersen SJ, Zandbergen HW, Holmestad R. Metall Mater Trans A 2005;36:691.
[5] Marioara CD, Nordmark H, Andersen SJ, Zandbergen HW, Holmestad R. J Mater Sci 2006;41:471.
[6] Vissers R, van Huis MA, Jansen J, Zandbergen HW, Marioara CD, Andersen SJ. Acta Mater 2007;55:3815.
[7] Andersen SJ, Marioara CD, Vissers R, Frøseth A, Zandbergen HW. Mater Sci Eng A 2007;444:157.
[8] Andersen SJ, Marioara CD, Frøseth A, Vissers R, Zandbergen HW. Mater Sci Eng A 2005;2005:127.
[9] Zandbergen HW, Andersen SJ, Jansen JE. Science 1997;277:1221.
[10] Matsuda K, Sakaguchi Y, Miyata Y, Uetani Y, Sato T, Kamio A, Ikeno S. J Mater Sci 2000;35:179.
[11] Derlet PM, Andersen SJ, Marioara CD, Frøseth A. J Phys Cond Matter 2002;14:4011.
[12] Pogatscher S, Antrekowitsch H, Leiner H, Sologubenko AS, Uggowitzer AS. Scr Mater 2013;68:158.
[13] Sha G, Möller H, Stumpf WE, Xia JH, Govender G, Ringer SP, Acta Mater 2012;60:692.
[14] Ehlers FJH, Comput Mater Sci 2014;81:617.
[15] Ninive PH, Strandlie A, Gulbrandsen-Dahl S, Lefebvre W, Marioara CD, Andersen SJ, Friis J, Holmestad R, Løvvik OM. Acta Mater 2014;69:126.
[16] Saito T, Wenner S, Osmundsen E, Marioara CD, Andersen SJ, Røyset J, Lefebvre W, Holmestad R., Philos Mag Accepted 2014 DOI:10.1080/14786435.2014.913819
[17] Pennycook SJ, Jesson DE. Phys Rev Lett 1990;64:938.
[18] Pennycook SJ. Adv Imag Elect Phys 2000;103:147.
[19] van Aert S, de Backer A, Martinez GT, Goris B, Bals S, van Tendeloo G. Phys Rev B 2013;87:064107.
[20] de Backer A, Martinez GT, Rosenauer A, van Aert S. Ultramicroscopy 2013;134:22.
[21] Koch CT. PhD. Thesis. Determination of core structure periodicity and point defect density along dislocations. Arizona State University, 2002.
[22] Gao HX, Peng LM. Acta Cryst A 1999;55:926.
[23] Hohenberg P, Kohn W. Phys Rev B 1964;136:864.
[24] Kohn W, Sham LJ. Phys Rev A 1965;140:1133.
[25] Vanderbilt D, Phys. Rev B 1985;32;8412.

[26] Kresse G, Hafner J, Phys Rev B 1993;47:558.
[27] Kresse G, Furthmüller J, Comput Mater Sci 1996;6:15.
[28] Perdew JP, Chevary JA, Vosko SH, Jackson KA, Pederson MR, Singh DJ, Fiolhais C. Phys Rev B 1992;46:6671.
[29] Monkhorst HJ, Pack JD. Phys Rev B 1976;13:5188.
[30] van Helvoort ATJ, Dahl Ø, Soleim BG, Holmestad R, Tybell T. Appl Phys Lett 2005;86:092907.
[31] Nellist PD, Pennycook SJ, Ultramicroscopy 1999;78:111.
[32] van Aert S, Batenburg KJ, Rossell MD, Erni R, van Tendeloo G. Nature 2011;470:374.
[33] Ehlers FJH, Dumoulin S, Marthinsen K, Holmestad R. Model Simul Mater Sci Eng 2013;21: 085018.
[34] Haruta M, Kurata H, Komatsu H, Shimakawa Y, Isoda S. Ultramicroscopy 2009;109:361.
[35] Findlay SD, LeBeau JM, Ultramicroscopy 2013;124:52.
[36] Glas F. Phys Rev B 1995;51:825.

Table 1 Structural overview and atomic site positions (x, y, z) in the β" phase [2, 3]. Each atomic site is schematically shown in Figure 1 (a).

Composition	$Mg_5Al_2Si_4$
Space group	C2/m
Lattice parameter (nm)	a=1.516, b=0.405, c=0.674, β = 105.3°
Mg1 site	0, 0, 0
Mg2 site	0.3419, 0, 0.099
Mg3 site	0.4225, 0, 0.659
Si1 site	0.0501, 0, 0.678
Si2 site	0.1876, 0, 0.225
Si3/Al site	0.2213, 0, 0.618

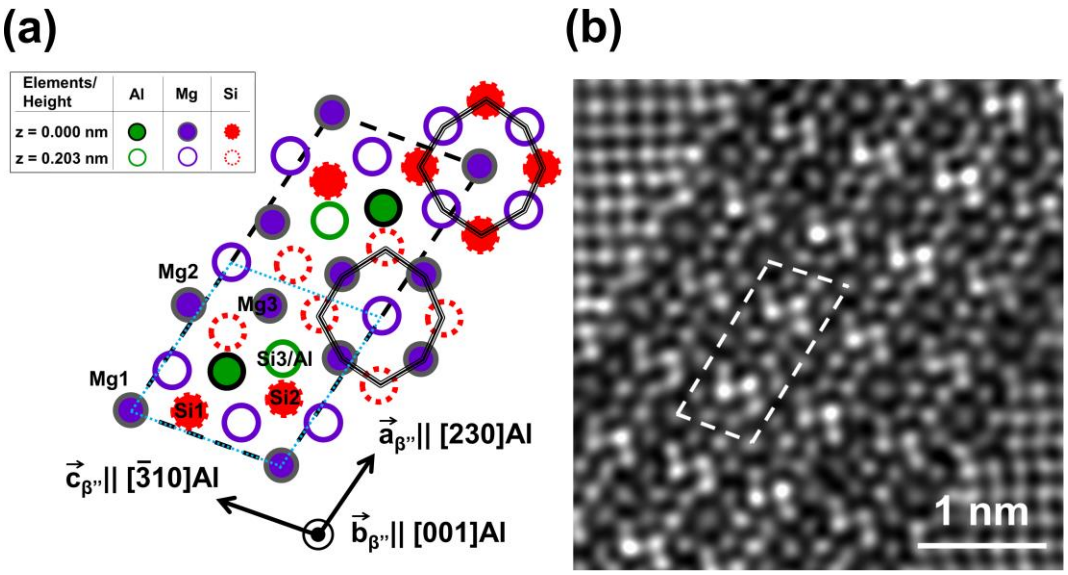

Figure 1 (a) Projected unit cell of the β" phase along the b-axis. The labelling of atoms refers to Table 1. The characteristic 4-fold atomic coordination around the Mg1 site is indicated by a triple solid black line. The dashed large boxes in (a, b) represent a unit cell and the dotted blue one in (a) shows the primitive cell used in DFT calculations. (b) HAADF-STEM image of a β" cross-section taken along <001>Al (same orientation as in (a)) for an alloy containing 0.42at.%Zn after isothermal heat treatment for 12 h at 185°C. The image has been filtered using Fast Fourier transform (FFT) with a circular band pass mask that removed all periods (noise) shorter than 0.15 nm (adopted from Ref. [16]).

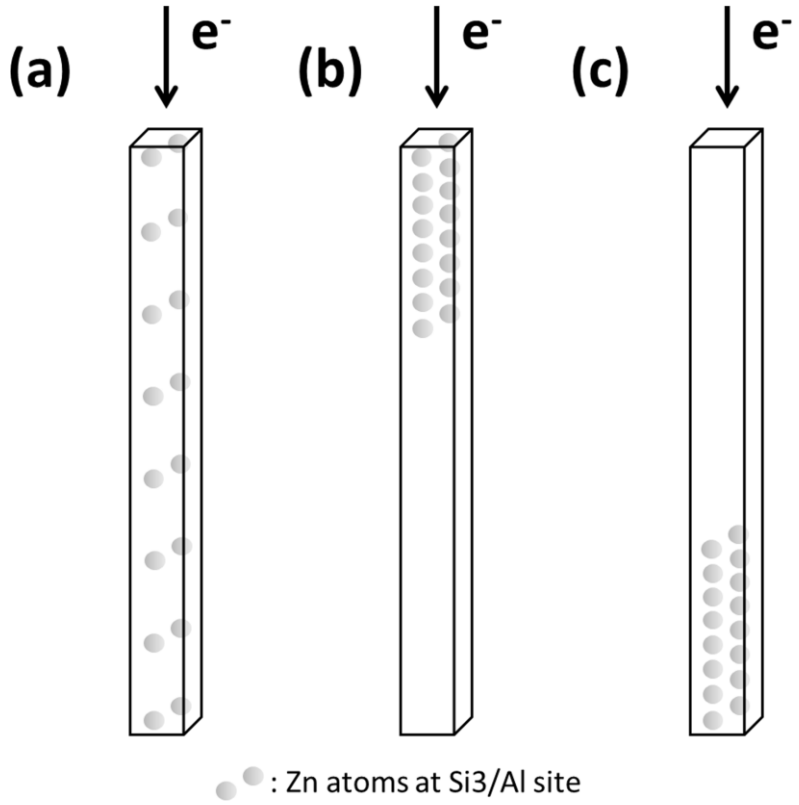

Figure 2 Schematic image of precipitate columns for different distributions of Zn along the electron beam direction: (a) even distribution of Zn atoms throughout the column, (b) top and (c) bottom Zn atom enrichments. The precipitate column represents one primitive β” unit cell (repeated along the b-axis).

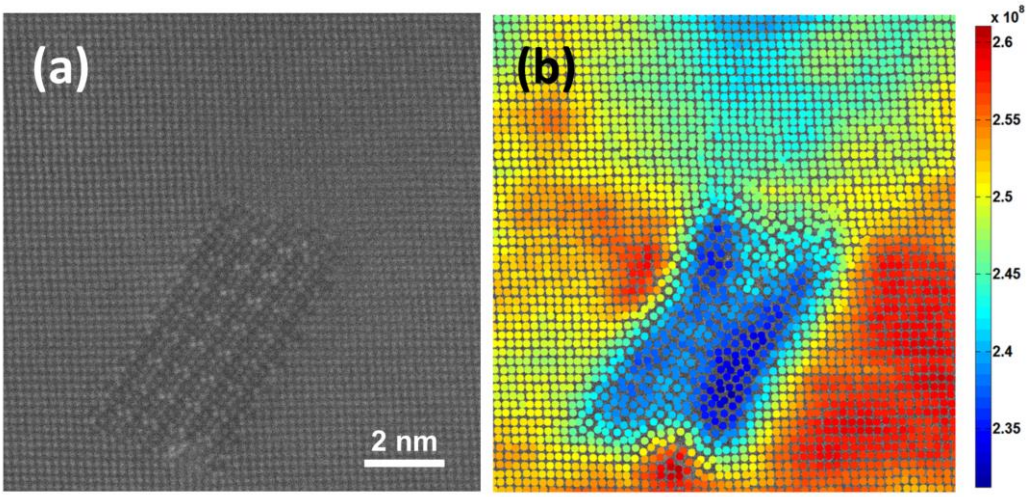

Figure 3 (a) Unprocessed HAADF-STEM image of a Zn-containing β" precipitate cross-section taken along <001>Al. (b) Corresponding HAADF-STEM intensity map. Each coloured dot overlaying an atomic column represents an integrated HAADF-STEM intensity of a square area of 1.25 x 1.25 nm^2 (i.e. much larger than the size of the projected column). The overlay therefore represents the average thickness variations for the specimen. The HAADF intensity is displayed in arbitrary units. The precipitate orientation is the same as in Figure 1 (a).

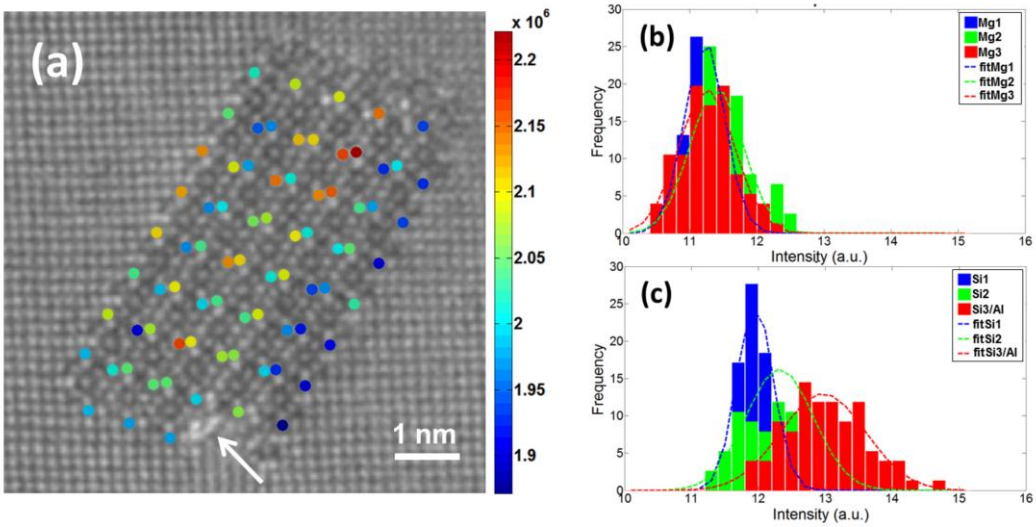

Figure 4 (a) Colour mapping of the integrated intensity on the Si3/Al sites of the Zn-containing β" precipitate. The HAADF-STEM intensity is displayed in arbitrary units. In (b) and (c), the respective intensity distributions for Mg and Si sites in the precipitate are shown. The columns at the bottom part of the precipitate had non-systematically higher intensity (shown by white arrow in (a)) and were excluded in the statistics of intensity distributions.

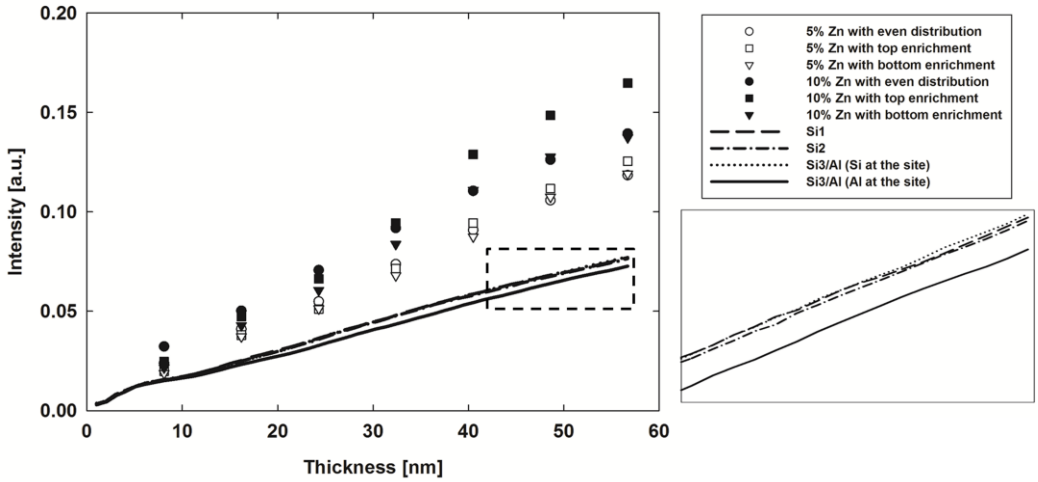

Figure 5 Simulated intensities of the Si3/Al site in the β" phase (points) as a function of specimen thickness for 5% and 10% Zn occupancies with different Zn distributions along the electron beam direction, as given in the legend. The composition of the β" phase was assumed to be $Mg_5Al_2Si_4$. As a reference (solid lines), the intensities of all Si sites (Si1, Si2 and Si3 sites) in the β" phase *without* Zn occupation (assuming the Mg_5Si_6 composition) are also shown, along with the intensity for Al on the Si3/Al site (assuming the $Mg_5Al_2Si_4$ or $Mg_4Al_3Si_4$ composition). See Table 2 for the estimated intensity gradients with thickness. The right bottom rectangle shows enlarged the dashed rectangle corresponding to thicknesses above 40 nm.

Table 2 HAADF-STEM intensity gradients as a function of specimen thickness, deduced by linear interpolation of selected datasets from Figure 5. The linear functions were fitted with zero intercept term, i.e. zero intensity at zero thickness is assumed.

Si3/Al sites	Gradient ($\times 10^{-3}$)
Without Zn occupation	1.3
5% Zn with even distribution	2.2
5% Zn with top enrichment	2.3
5% Zn with bottom enrichment	2.1
10% Zn with even distribution	2.6
10% Zn with top enrichment	3.0
10% Zn with bottom enrichment	2.5

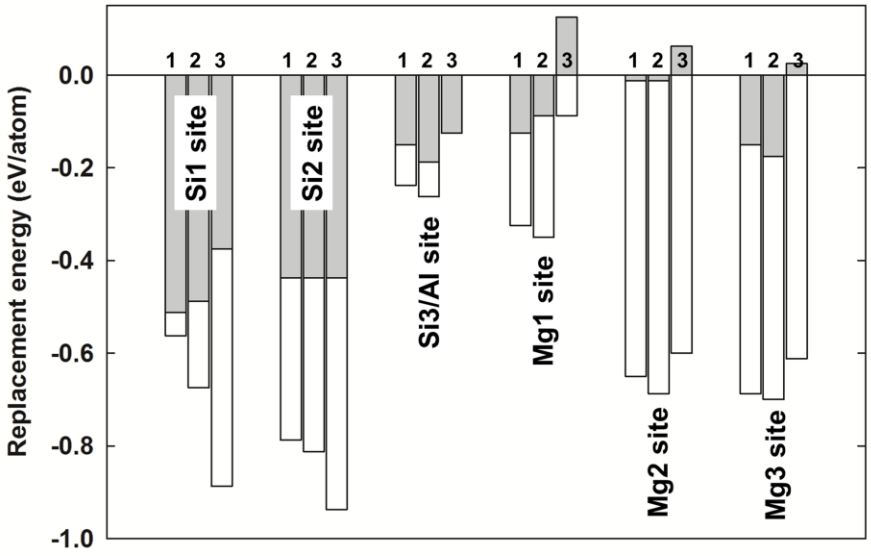

Figure 6 Calculated replacement energies for Zn and alternative solute atoms Mg/Si on the different sites of three different β" configurations. 1: $Mg_4Al_3Si_4$, 2:$Mg_5Al_2Si_4$ and 3: Mg_6AlSi_4. Zn and Mg/Si replacement energies are labelled with grey and white bars, respectively. Mg was incorporated for comparison with Zn on the Si3/Al site.

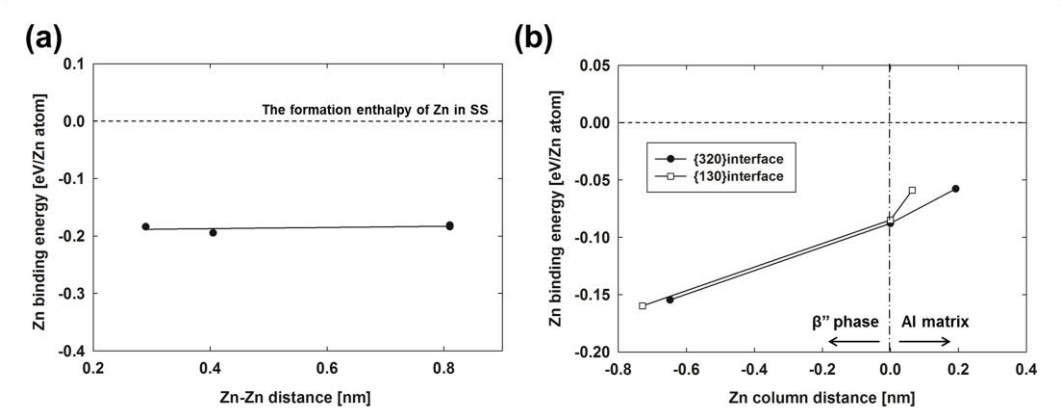

Figure 7 Zn binding energies at the Si3/Al site as a function of (a) distance between the Zn atoms along the precipitate needle direction, and (b) the column distance from the interfaces. Zero energy denotes the formation enthalpy of isolated Zn in SS. In (b), the zero value on the x-axis represents the first Si3/Al site at the interface [14] and negative and positive values correspond to β" bulk side and Al matrix side, respectively.